

On the origin of the 13 μm feature^{*}

A study of ISO-SWS spectra of oxygen-rich AGB stars

T. Posch¹, F. Kerschbaum¹, H. Mutschke², D. Fabian², J. Dorschner², and J. Hron¹

¹ Institut für Astronomie, Türkenschanzstrasse 17, 1180 Wien, Austria

² Astrophysikalisches Institut und Universitätssternwarte, Schillergässchen 2–3, 07745 Jena, Germany

Received 2 September 1999 / Accepted 18 October 1999

Abstract. We have derived a mean profile of the 13 μm emission feature from 11 ISO spectra of oxygen-rich AGB stars and present an overview of the mineral species that could account for it. Our results can be summarized as follows: i) Spherical particles of $\alpha\text{-Al}_2\text{O}_3$ (corundum) have a sharp emissivity maximum peaking at 12.7 μm . The difference of 0.3 μm in the peak position compared to the mean observed band profile is a serious obstacle to assigning the 13 μm dust feature to this dust species. ii) From a continuous distribution of ellipsoidal $\alpha\text{-Al}_2\text{O}_3$ -particles, a broad emissivity profile peaking at 13–14 μm emerges. It is difficult to reconcile the large width of this profile with the width of the observed 13 μm band. iii) The most prominent emissivity maximum of TiO_2 (rutile) is located at 13.5 μm ; its width is larger and its strength three times smaller than the emissivity maximum of corundum. iv) Core-mantle-grains composed of rutile and corundum or of corundum and amorphous olivine can both produce, in a certain domain of core volume fractions, a spectral signature very similar to the observed 13 μm feature. However, the necessity to assume rather artificial distribution functions of the core volume fractions makes this scenario improbable. v) We consider MgAl_2O_4 (spinel) to be the most promising candidate for the carrier of the 13 μm feature since its emissivity peaks are located at 12.95 μm and at 16.8 μm for spherical particles and since at *both* positions features are present in most of the spectra of our sample. In view of the relevance of this substance for circumstellar shells, laboratory spectra of spinel particles embedded in KBr are also presented.

Key words: stars: variables: general – stars: AGB and post-AGB – stars: circumstellar matter – stars: mass-loss – infrared: stars

1. Introduction

Whereas amorphous silicates are known to be constituents of circumstellar dust since the 1970 s, it was not before the end of

Send offprint requests to: T. Posch (posch@astro.univie.ac.at)

^{*} Based on observations with ISO, an ESA project with instruments funded by ESA Member States (especially the PI countries: France, Germany, the Netherlands and the United Kingdom) and with the participation of ISAS and NASA.

the 1980 s that a dust feature in the spectra of oxygen-rich AGB stars was with some constancy ascribed to another kind of solid particles. Hackwell (1972) was among the first authors to point out that silicates might not be the only kind of dust with spectral signatures in the 8–13 μm region. Onaka et al. (1989) tentatively identified a broad feature at 12–13 μm observed in IRAS-LRS spectra as a band feature of partially crystallized γ -aluminum oxide particles. They noted that the 12–13 μm feature is prominent especially when the asymmetry factor of the visual light curve is large. Sloan et al. (1996) presented an analysis of 187 LRS spectra in which the 13 μm feature is present. They came to the result that 75–90 % of all SRb variables but only 20–25 % of the Miras with oxygen-rich dust show the 13 μm feature. As a possible explanation for this fact, they proposed that the absence or weakness of pulsational shock waves allows the carrier of the 13 μm feature to form and survive. More recently, Sloan & Price (1998) suggested that there may be a correlation between the presence of alumina grains and a star's C/O ratio, such that in case of a C/O ratio close to unity, almost all oxygen will be consumed by alumina grains, whereas in case of smaller C/O ratios, an increasing amount of silicates will form. Hron et al. (1997) found that the 13 μm feature is observed in stars within a rather narrow range of photospheric and dust shell temperatures, indicating that the formation of its carrier strongly depends on the physical conditions inside the circumstellar shell.

Begemann et al. (1997) derived an average band profile of the 13 μm feature from 51 IRAS-LRS-spectra and compared it with the opacities of various forms of aluminum oxides. They pointed out that both amorphous and $\gamma\text{-Al}_2\text{O}_3$ cannot account for the 13 μm feature, whereas $\alpha\text{-Al}_2\text{O}_3$ can, if a continuous distribution of ellipsoidal grain shapes is assumed. Kozasa & Sogawa (1997) discussed the formation of heterogeneous grains composed of a corundum core and a silicate mantle. They argued that the condensation of silicates on pre-condensed Al_2O_3 is the natural process of dust formation and presented radiative transfer calculations according to which a feature at 13–14 μm attributed to Al_2O_3 appears if the mass loss rate of an oxygen-rich AGB star is below $2 \times 10^{-5} M_{\odot}$. In contrast to these authors, Gail & Sedlmayr (1998) and Jeong et al. (1999) found that Al_2O_3 is very unlikely to be a condensation seed in O-rich circumstellar shells. According to their calculations, TiO_2 should be the very first condensate in M star envelopes.

On the basis of our previous work (Posch & Kerschbaum 1999), we try here to give an overview of the mid-IR opacities of dust species (the optical constants of which are given in the literature) that could account for the 13 μm feature. All of the substances considered here show, apart from an emissivity peak near 13 μm , additional major or minor spectral signatures. Their positions and relative strengths are discussed, because we consider them essential for a unique identification, which is not possible on the basis of the 13 μm band alone.

2. Observational data

2.1. The sample of ISO spectra

The Semiregular variables of types SRa and SRb (SRV) and the Irregular variables of type Lb (IRV) are quite numerous groups of objects among the stars on the AGB. They can provide important constraints on theoretical mass-loss models due to their pulsational behaviour in which they differ from the more frequently studied Mira variables. In a series of papers (Kerschbaum & Hron 1992, 1994, 1996; Kerschbaum 1995; Hron et al. 1997) the SRVs have been studied in a systematic way.

The SRVs are known since the end of the 1980s to show prominent 13 μm emission features. The availability of high quality ISO data was the starting point of this investigation.

We used data from 5 open time ISO projects (*fker-schb.orichsrv/orichsrl/zzagb2pn*; *jhron.varlpv/varlpv2*) for our work. In these programmes we tried on one hand to cover representative O-rich AGB variables with different pulsational properties (Mira, SRa, SRb, Lb, and OH/IR) and on the other hand to monitor a few objects in order to study the spectral changes. In total we were able to observe 22 objects at least once. For this paper we selected a subset of spectra with strong 13 μm emission; because of the type of the corresponding stars (SRb), the stellar variability plays a minor role here (Kerschbaum et al. 1999). No clear indications for time variations of the 13 μm feature were found in case of the stars for which we have two spectra.

Additional spectra were taken from the ISO data archive. They originate from the projects *sprice.startyp1*, *sprice.startyp2* and *jgoebel.oxystars*.

Our observations were carried out with ISO-SWS (de Graauw et al. 1996) with full grating scans (2.4 μm to 44 μm , AOT01 and speed 2, typically) and an intrinsic resolution between 400 and 600. The pipeline processed data products (OLP 7.+) were further reduced with ISAP. The connection of the individual bands which introduces an additional uncertainty was done by multiplying the longer wavelength band in order to fit overlapping regions. For flux levels below 100 Jy the correction was applied additively. Fig. 1 shows the reduced spectra in the wavelength range from 11.5 to 17.5 μm on which we are focussing here.

Table 1 lists the properties of the stars of our sample. All of the stars on which this work is based are Semiregulars of type SRb. Their mass-loss-rates are comparatively small, i.e. below $3 \times 10^{-7} M_{\odot}$ in all cases where they are known.

Data on the gas mass-loss are adopted from Kerschbaum et al. (1996), Kahane & Jura (1994) and Knapp et al. (1998). RV Boo (Kerschbaum et al. 1997, Bergmann et al. 1999) and EP Aqr (Knapp et al. 1998) show very peculiar CO lineshapes and have probably a complex, nonspherical distribution of their circumstellar material.

2.2. Deriving the 13 μm band profile

To derive an average 13 μm band profile from our spectra, we used a method similar to the one described by Begemann et al. (1997). We fitted a fifth-degree polynomial to each spectrum in the wavelength ranges 10.0–12.25, 14.2–14.8, 15.1–15.3, 15.55–16.1, 16.25–16.6 and 17.3–18 μm , thus skipping the range of the 13 and 17 μm emissions as well as the CO₂ emission lines (see Justtantont et al. 1998). Using polynomials of higher degree did not improve the quality of the fits. The least square fits were subtracted from the original spectra to get the individual 13 μm band profiles. These individual profiles were then normalized and summed up (with equal statistical weight). In Fig. 2 the normalized individual residuals are plotted, whereas Fig. 3 shows the result of summing them up. Apart from the 13 μm band, five sharp emission lines at 13.48, 13.87, 14.97, 15.40 and 16.18 μm can be seen. These lines are due to rovibrational transitions of CO₂ molecules. Furthermore, a rather weak feature at 16.8 μm can be seen. This feature coincides in position and relative strength with a minor emissivity maximum of spinel (see Sect. 3.2 and Fig. 14). There may be an additional feature at 15.8 μm for which we cannot, however, suggest an identification.

2.3. Position and width of the 13 μm feature

The most striking property of the 13 μm band is its small width compared to the width of the 10 and the 17–18 μm silicate features. This was already evident from previous work based on IRAS spectra. Sloan et al. (1996) found a full width at half maximum (FWHM) value of about 0.6 μm ; Begemann et al. (1997) report a value of 1.05 μm . (The corresponding widths of the 10 and the 17–18 μm silicate feature are, according to Dorschner et al. (1995), 1.6–2.6 μm and 6–7.5 μm , respectively.)

In order to determine the positions and widths of the 13 μm feature for the individual spectra, we used the following method: a second degree parabola was fitted to each of the residual emission profiles in the wavelength range 12.5–13.4 μm . The highest point of the respective parabola (and not the highest point of the spectrum, the position of which is determined by noise) was considered to represent the peak of the feature. To derive the FWHM value, we used the same parabola. The results are listed in the last two columns of Table 1. For the stars of which we have two spectra, we give mean values. The band position is between 12.95 and 13.05 μm and the FWHM amounts 0.5–0.8 μm . It should be noted, though, that the latter value is a result of a contamination of the 13 μm feature with the 13.48 μm CO₂ line in case of the spectra of T Sge and V 438 Oph. This contamination

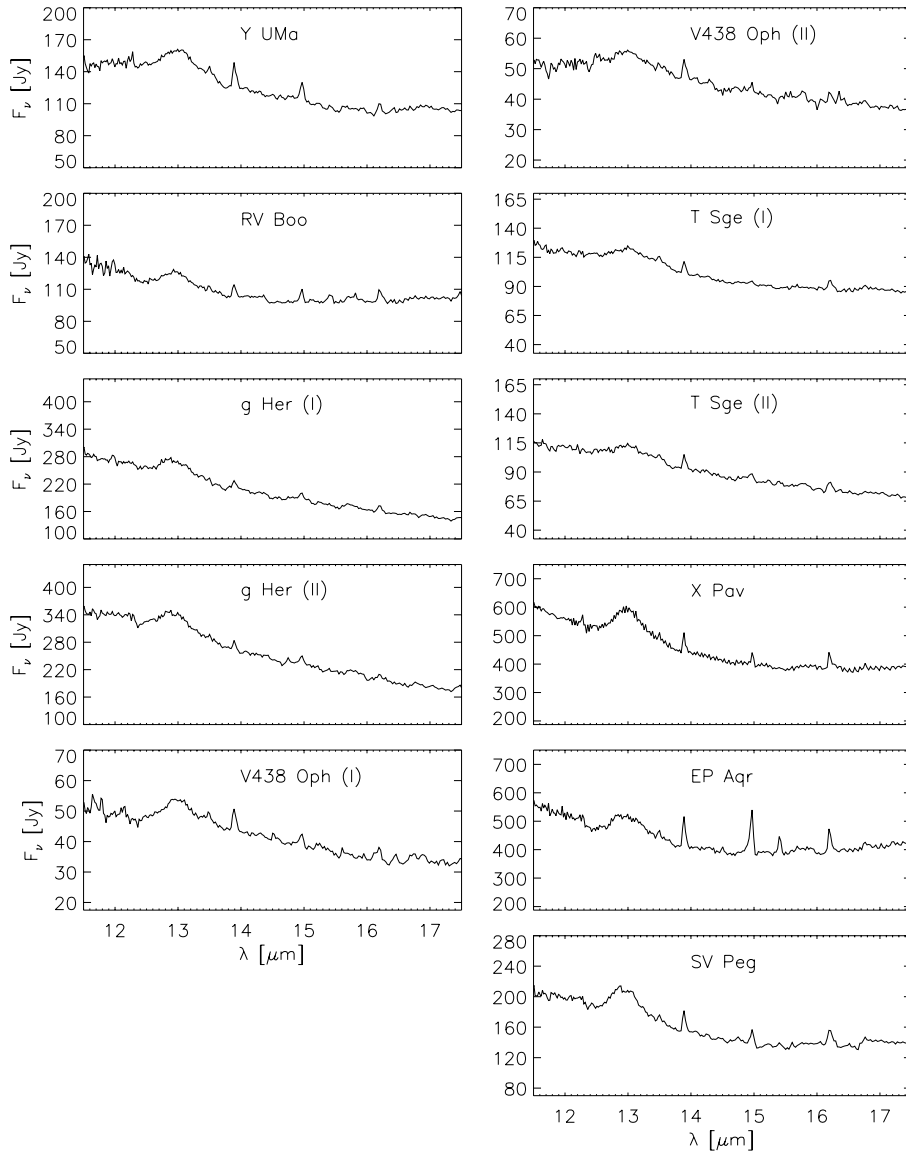


Fig. 1. The reduced ISO spectra.

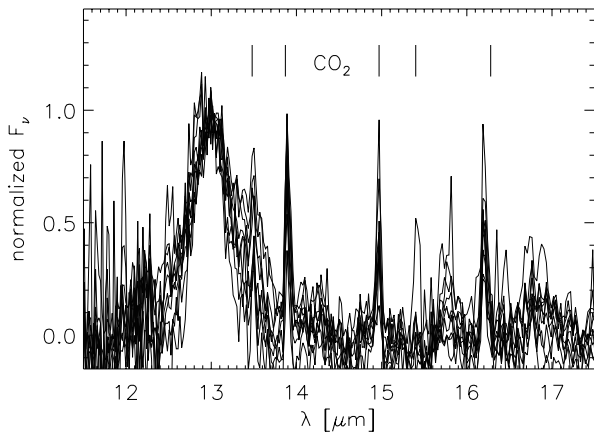


Fig. 2. The normalized individual residual emission profiles in the 12–17 μm range, derived by subtraction of a fifth order polynomial from our spectra.

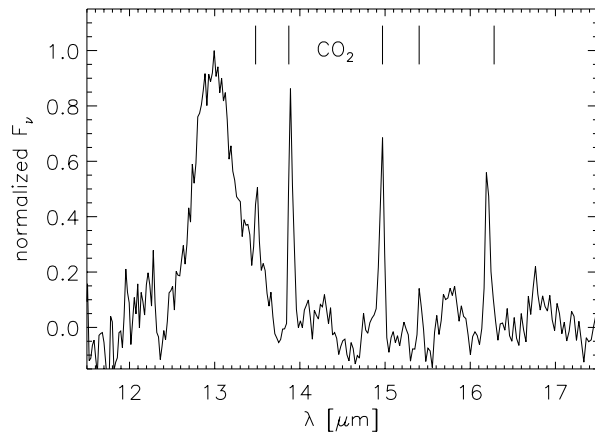


Fig. 3. The average residual emission profile in the 12–17 μm range, derived by summing up the normalised individual residuals shown in the previous figure.

Table 1. Properties of the sample stars

Name	IRAS Name	Type	Period [d]	Spectrum	LRS	F_{12} [Jy]	v_{exp} [km s $^{-1}$]	dM/dt [M_{\odot}/yr]	band position [μm]	FWHM [μm]
Y UMa	12380+5607	SRb	168	M7II-III:	15	192.6	5	2×10^{-7}	13.0	0.7
RV Boo	14371+3245	SRb	137	M5e-M7e	22	125.0	7	2×10^{-7}	13.0	0.5
g Her	16269+4159	SRb	89	M6III	16	437.6	9	1×10^{-7}	12.95	0.6
V438 Oph	17123+1107	SRb	170	M0-M7e	15	61.6			13.0	0.75
T Sge	19194+1734	SRb	166	M4-M6.5	15	140.2			13.05	0.8
X Pav	20075-6005	SRb	199	Mc	22	556.8			13.0	0.6
EP Aqr	21439-0226	SRb	55	M8III	23	637.4	10	2×10^{-7}	13.0	0.6
SV Peg	22035+3506	SRb	145	M7	21	264.7	8	3×10^{-7}	12.95	0.6

may also be the reason for the comparatively large feature width found by Begemann et al. (1997).

3. Possible identifications of the 13 μm feature

We will now present possible carrier substances of the 13 μm feature, the optical constants of which are listed in reference books (mainly Palik 1985-98). Both for spherical particle shapes and for a continuous distribution of ellipsoids (CDE), we calculated the volume normalized absorption cross section C_{abs}/V , which also determines the emissivity (since in thermodynamic equilibrium, absorption is balanced by emission). V designates the mean particle volume in both cases. For circumstellar shells that are optically thin (which is the case for all the stars of our sample), the emission of each dust component can be, to a reasonable approximation, calculated by multiplying C_{abs} with an integral over Planck functions for the whole temperature range of the shell (see e.g. Onaka et al. 1989). A more sophisticated approach would be of course to use C_{abs} together with a grain size distribution as an input parameter for a radiative transfer calculation. However, since we are mainly interested here in the 13 μm feature, i.e. in dust emission from a rather limited wavelength range, we will not present model spectra for the dust shells, but only compare the residual emission profile derived by the method described in Sect. 2 with C_{abs} -profiles. It is clear that both profiles or functions do not represent exactly the same physical quantity; but there is a close interrelation between both such that C_{abs} governs the peak positions and widths of the dust emission (unless, as mentioned, the circumstellar shell is optically thick).

Sects. 3–4 are structured as follows. We first present the emissivity of corundum, because it is most often made responsible for the 13 μm feature. Second, the optical properties spinel of (MgAl_2O_4), which can be considered as an MgO-containing alumina species, are discussed. Third, the spectral signature of titanium dioxide is confronted with the observed 13 μm band profile. Finally, after arguing against Speck’s (1998) hypothesis that SiO_2 could account for the 13 μm feature, we sum up the results of our Mie calculations for core-mantle-grains.

3.1. $\alpha\text{-Al}_2\text{O}_3$ (corundum)

Corundum is a crystalline form of Al_2O_3 with rhombohedral lattice structure. The optical constants n and k must therefore

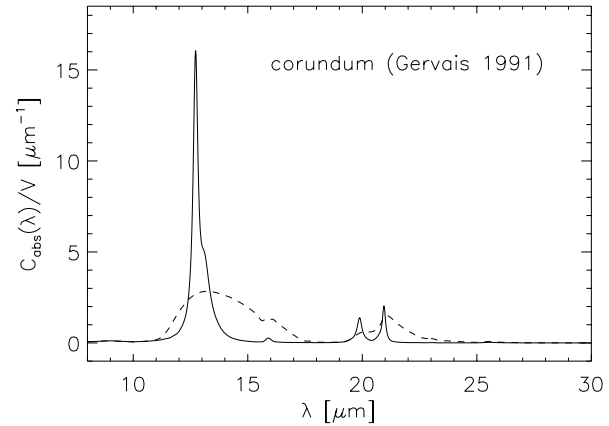


Fig. 4. The mid-IR emissivity of corundum. The full line denotes spherical particles, the dashed one a continuous distribution of ellipsoids (CDE).

be measured for two principal polarizations of the incident light, namely for parallel and for perpendicular polarization. The light beam polarized perpendicularly to the crystal’s symmetry axis is called the ordinary ray, the one with parallel polarization is called the extraordinary. The corresponding values of C_{abs} will be named $C_{abs,o}$ and $C_{abs,e}$ in the following. Since we assume the particles to be randomly oriented in circumstellar environments, a proper mean of those two values has to be calculated. This mean is given by

$$C_{abs} = \frac{2}{3}C_{abs,o} + \frac{1}{3}C_{abs,e}, \quad (1)$$

because there are *two* orthogonal directions in space which are both perpendicular to the crystal’s symmetry axis, but only *one* being parallel to it.

In Fig. 4, the mid-IR profile of C_{abs}/V of $\alpha\text{-Al}_2\text{O}_3$ is presented for two different cases: for spherical particles on the one hand and for a CDE on the other hand. In both cases, the particles were assumed to be small compared to the wavelength and the most recent data set was used. This data set is due to Gervais & Piriou (1974, 1975) and was taken from Gervais (1991), where it is listed together with the results of Barker (1963), which yield a similar emissivity profile. For spherical particles, we used Mie theory to calculate $C_{abs,o}$ and $C_{abs,e}$ from n_o , k_o , n_e and k_e , respectively, and derived the mean value C_{abs} according to Eq. (1). For the ellipsoidal particles, we adopted the shape

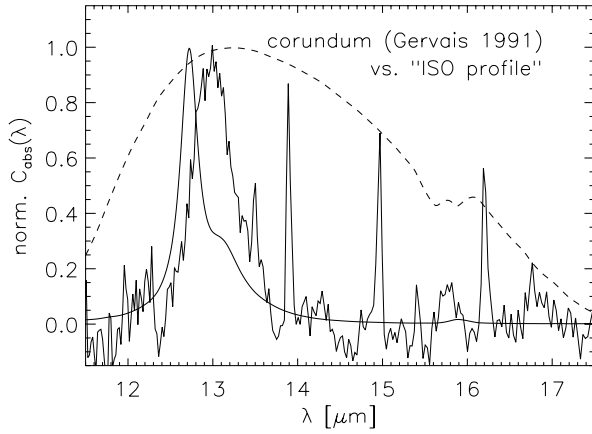


Fig. 5. The mid-IR emissivity of corundum. The full line denotes spherical particles, the dashed one a CDE. For comparison, the residual emission profile that we have derived from the ISO spectra is also shown.

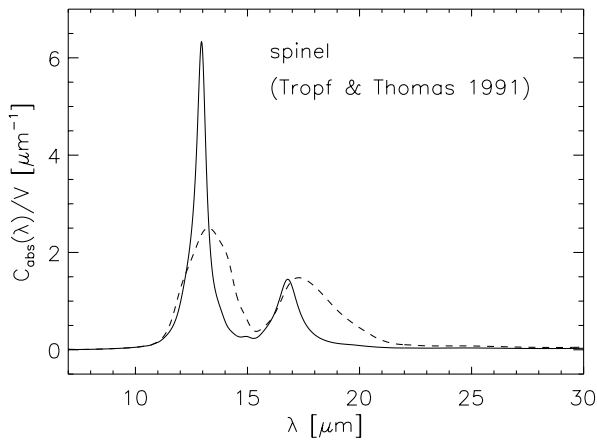


Fig. 6. The mid-IR emissivity of spinel. The full line denotes spherical particles, the dashed one a CDE.

distribution described by Ossenkopf et al. (1992) which is based on the general concept of Bohren & Huffman (1983). Note that the maximum value of C_{abs}/V in case of spherical particles, situated at $12.72 \mu\text{m}$, amounts about $16.5 \mu\text{m}^{-1}$, which is about six times larger than in the CDE case and more than 30 times larger than for a typical amorphous astronomical silicate (see e.g. Ossenkopf et al. 1992). This implies that for approximately spherical particles small amounts of corundum (a few percents) may be sufficient to produce a feature comparable in strength to the $10 \mu\text{m}$ silicate band. Qualitatively, the same is true for spinel and rutile, as can be seen from Figs. 6 and 8, even though their maximum C_{abs}/V values are about three times smaller.

In Fig. 5, we have normalized the values of C_{abs} such that the maximum value equals unity and overplotted the residual profile shown in Fig. 3. It is evident from this figure that

(a) the emissivity profile of spherical $\alpha\text{-Al}_2\text{O}_3$ -particles peaks at a wavelength $0.3 \mu\text{m}$ smaller than the $13 \mu\text{m}$ dust feature; but
(b) the FWHM value of the observed feature agrees quite well with the FWHM of corundum spheres, whereas it is about 7 times smaller than it would be in case of the assumed CDE.

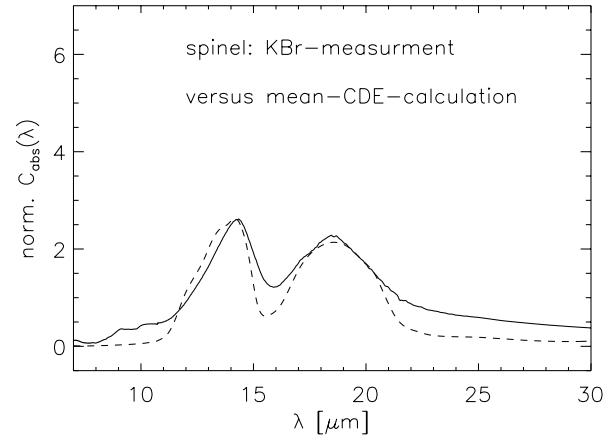


Fig. 7. Absorption spectra of spinel: laboratory measurement of particles embedded in KBr (solid line) compared to a CDE calculation for particles in KBr (dashed). ‘Mean CDE’ designates a continuous distribution of ellipsoids with equal probability for all shapes (from needles to disks).

However, a CDE with a shape distribution function giving even stronger preference to spheres would result in a smaller FWHM.

Minor maxima of C_{abs}/V are located at 20 and at $21 \mu\text{m}$.

It should be mentioned that Gervais (1991) also reports a data set for a polycrystalline sample of hot-pressed 99.9% alumina for which the maximum of C_{abs} is situated at $13 \mu\text{m}$ instead of $12.7 \mu\text{m}$, as for the measurements of $\alpha\text{-Al}_2\text{O}_3$ -samples. However, this may be due to the fact that the author of this data set, Worrell (1986), only presents rather low resolution reflectance spectra (no table of n and k), from which the optical constants were then deduced. We don’t think it would be justified to trust these particular data only because they better match the $13 \mu\text{m}$ dust feature.

3.2. MgAl_2O_4 (spinel)

Magnesium aluminum spinel is a cubic mineral, the composition of which can be written as $\text{MgO} \times m\text{Al}_2\text{O}_3$, with m varying between 0.9 and 4. Its melting point is approximately 2400 K, i.e. about 100 K above the one of corundum (Tropf & Thomas 1991). Gail & Sedlmayr (1998) found that with decreasing temperature, the stability of MgAl_2O_4 exceeds the one of Al_2O_3 and that an almost sudden transition from corundum to spinel can take place in chemical equilibrium.

Nittler et al. (1997) listed spinel among the presolar oxide grains which have been found in meteorites (however, only a small fraction of those oxide grains are spinels, the majority of them being corundum particles).

To derive the emissivity of spinel, we have used the optical constants published by Tropf & Thomas (1991). They refer to stoichiometric spinel, i.e. to the case of $m = 1$ in the general formula given above. Due to the cubic crystal structure of spinel, no anisotropy in C_{abs} occurs. Fig. 6 shows the result of our calculations. Two peaks in C_{abs} can be seen, one at $12.95 \mu\text{m}$ with $C_{abs}/V = 6.4 \mu\text{m}^{-1}$ and a FWHM of $0.9 \mu\text{m}$ plus a second, four times weaker one at $16.8 \mu\text{m}$ with a FWHM of $1.5 \mu\text{m}$ (for

spherical particles). Whereas the first signature is due to Al-O-stretching vibrations, the second originates from the MgO content of spinel. A spectral signature similar to the latter but situated at longer wavelengths (17.7–19.9 μm) is characteristic of Mg-Fe-oxides (see Henning et al. (1995) for the optical constants and Bagnulo (1996) for radiative transfer calculations based on them).

For ellipsoidal particles, both emissivity peaks of spinel appear broader and are shifted by about 0.5 μm towards longer wavelengths. Note that in the case of spinel, especially, it was necessary to perform a cubic spline interpolation of the measured n and k values, because the wavelength grid of the data to which we refer is rather coarse. Measurements of small particles produced by grinding a stoichiometric Mg spinel yield absorption properties which are comparable to the case of a CDE calculation for a uniform shape distribution according to Bohren & Huffman (1983) (see Fig. 7). As is known for various other kinds of substances, the ground particles strongly deviate in their shape from spherical symmetry due to agglomeration. This effect – in combination with the presence of the KBr matrix – shifts the peak positions towards the red. Compared to spherical particles in vacuum, the shift amounts 1 μm in case of the 13 μm band and 2 μm in case of the 16.8 μm band. Therefore, if spinel is the carrier of the astronomical 13 μm feature, the particles must be approximately spherical, which is a reasonable assumption, though. For a detailed discussion of shape effects on the spectrum of ground particles see Henning & Mutschke (1999).

Unfortunately, most of the ISO spectra on which this work is based have a flux level which is rather low in the 15–20 μm region. However, the average residual emission presented in Sect. 2 does show, as we pointed out, a spectral signature at 16.8 μm (see Figs. 2, 3 and – for a comparison with laboratory data – Fig. 14).

An ongoing analysis of ISO archive spectra gives additional evidence for the presence of a spectral signature at 16.8 μm in sources of the 13 μm feature. We are planning to verify on the basis of a larger sample of spectra whether there is a clear correlation between the strengths of both features, which would give strong support to our hypothesis that they have the same origin.

3.3. TiO_2 (rutile)

Since TiO is known to be a rather abundant molecule in the atmospheres of M stars and since titanium oxides are stable up to high temperatures, these are considered as candidates for the first condensation products in circumstellar shells (see Gail & Sedlmayr 1998 and Jeong et al. 1999). On earth, the most abundant titanium oxide is the tetragonal rutile. Fig. 8 shows the emissivity of spherical and ellipsoidal rutile particles, calculated from the optical constants published by Ribarsky (1985). For this calculation, again, a mean of C_{abs} had to be derived according to Eq. (1). Three maxima of C_{abs} are present: the most prominent one is located at 13.5 μm and is comparable in strength to the principal emissivity maximum of corundum;

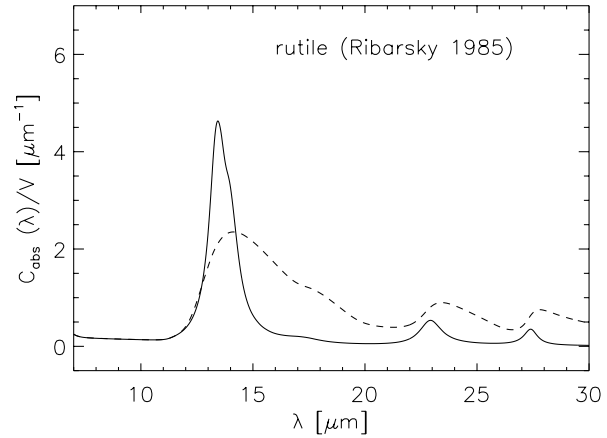


Fig. 8. The mid-IR emissivity of rutile.

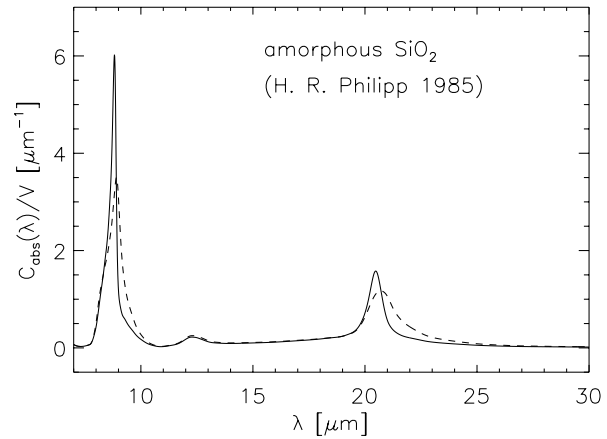


Fig. 9. The mid-IR emissivity of amorphous SiO_2 .

the other two maxima, both weaker by a factor of about 10, are situated at 23 and 27.5 μm . As in case of corundum, these minor spectral signatures could not be identified in the ISO spectra.

If we assume a CDE, the maxima of C_{abs} are again situated at even longer wavelengths, the principal one, for example, at 14 μm (see Fig. 8). Measurements which were not performed on single crystals, but on particles, also yield a broad main maximum of C_{abs} located at 14–16 μm (see e.g. Koike & Shibai 1998).

The only possibility to shift the maximum of C_{abs} towards shorter wavelengths is to ‘build’ a core-mantle-grain composed of TiO_2 and $\alpha\text{-Al}_2\text{O}_3$ (see Sect. 4.1).

3.4. Amorphous SiO_2 and Na-Al-silicates

Amorphous silicon dioxide (glass) exhibits three principal emissivity maxima: the most prominent one is situated at 8.9 μm , a second one at 20.5 μm , and a third, least prominent one at 12.3 μm (see Fig. 9; a similar plot is shown in Henning & Mutschke 1997, based on measurements made at the Jena laboratory). Speck (1998) suggested to attribute the feature at 12.5–13.0 μm observed by her with UKIRT in the spectra of O-rich AGB-stars to some form of SiO_2 . Among the possible identi-

fications discussed here, this one seems least probable to us, since

(a) if SiO_2 were responsible for the 13 μm feature, this feature should always be accompanied by even stronger 9 and 20.5 μm bands, which is not the case;

(b) the disagreement in band position (12.3 vs. 13 μm) is even more pronounced for SiO_2 than for $\alpha\text{-Al}_2\text{O}_3$.

This does not mean, of course, that we do not expect SiO_2 to be present at all in circumstellar dust.

A recent study by Mutschke et al. (1998) of aluminum silicates shows that incorporation of aluminum can shift the 12.3 μm SiO_2 feature to 13 μm and to even longer wavelengths (see the sodium-aluminum-silicate absorption spectra in Fig. 3 of Mutschke et al. 1998). However, in this case the width of the respective bands is too large compared to the observed 13 μm feature ($> 2 \mu\text{m}$ vs. $0.6 \mu\text{m}$). Furthermore, argument (a) also applies to these materials. Nevertheless, aluminum silicates may very well contribute to the continuum opacity in the trough between the 10 and 17–18 μm silicate bands.

4. Core-mantle-grains

4.1. Corundum-olivine

Core-mantle-grains composed of corundum and silicates were proposed by Kozasa & Sogawa (1997) as possible carriers of the 13 μm feature. According to these authors, corundum is the prime condensate in circumstellar outflows and serves as condensation nucleus for silicates. In their scenario, stars with $\dot{M} < 2 \times 10^{-5} M_\odot$ should show an emission feature ‘around 13–14 μm ’, whereas stars with higher mass loss are dominated by pure silicate features.

To calculate C_{abs} for core-mantle-grains, we used two methods. The simplest one is the so-called Maxwell-Garnett-formula. It allows to calculate an effective dielectric function ε of a core-mantle-grain small compared to the wavelength from the dielectric function ε_c of the core, the dielectric function ε_m of the mantle and the core volume fraction f :

$$\frac{\varepsilon - \varepsilon_m}{\varepsilon + 2\varepsilon_m} = f \frac{\varepsilon_c - \varepsilon_m}{\varepsilon_c + 2\varepsilon_m} \quad (2)$$

From this effective dielectric function ε , the quantity C_{abs}/V can be calculated from ε exactly in the same way as for one-component-particles:

$$\frac{C_{abs}}{V} = \frac{6\pi}{\lambda} \Im \left(\frac{\varepsilon - 1}{\varepsilon + 2} \right) \quad (3)$$

A second, independent method to calculate the emissivity of core-mantle-grains is using existing Mie codes. We adopted the programme BHCOAT, which was developed by Bohren & Huffman (1983). In the Rayleigh limit ($2\pi a \ll \lambda$ and $|\sqrt{\varepsilon}| 2\pi a \ll \lambda$), BHCOAT and Eqs. (2) & (3) are equivalent.

The resulting values of C_{abs}/V for core-mantle-grains composed of corundum and amorphous olivine (after Dorschner et al. 1995) are shown in Fig. 10 for different values of f . In this figure, we limited f to values up to 0.1, since if it is larger,

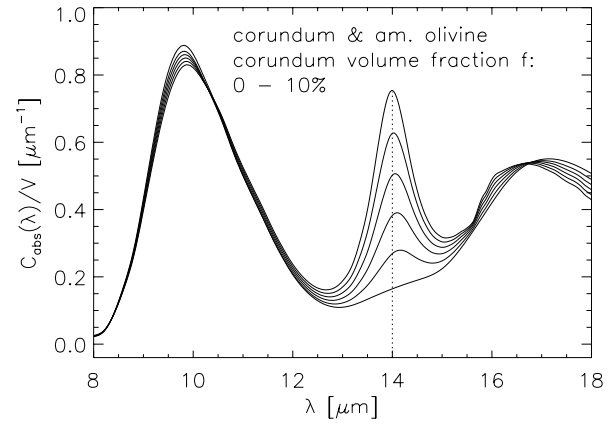


Fig. 10. The absorption efficiency of core-mantle-grains composed of corundum and amorphous olivine. The peak position of the feature corresponding to a volume fraction of the corundum core of 10% is 14.0 μm .

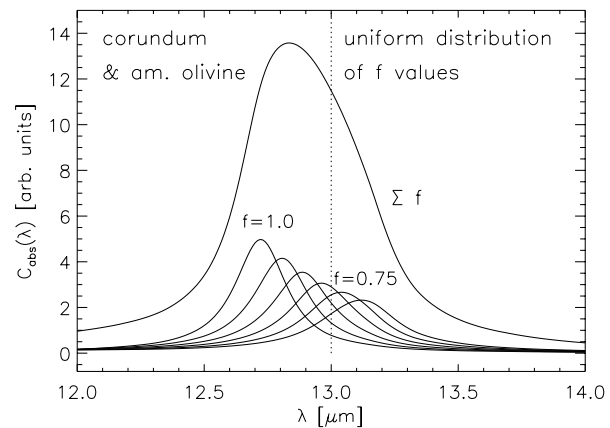


Fig. 11. The absorption efficiency of core-mantle-grains composed of corundum and amorphous olivine, the core volume fraction being uniformly distributed between 100 and 75%. The curves at the bottom of the figure show the (equally weighted) C_{abs} -profiles that were summed up to derive curve ‘ Σf ’.

the resulting relative strength of the corundum emission is unrealistically large compared to the observations. For this core volume fraction domain, the 12.7 μm corundum band is shifted to 14 μm and beyond.

In spite of this, one could think of a scenario which would produce the observed 13 μm feature. If a large population of pure silicate grains is present (regardless of the way they have formed), then an additional population of core-mantle grains with uniformly distributed values of f will produce a feature peaking near 13 μm which is *not* necessarily stronger than the silicate bands. Fig. 11 shows this situation, focussing on the 13 μm band only. To derive the emissivity profile designated by Σf , the C_{abs}/V -values for different corundum core volume fractions ($0.1 \leq f \leq 1$) were summed up. Though in this sum all terms were given the same statistical weight, the terms corresponding to high f values dominated, reflecting the much higher C_{abs} -values of corundum compared to amorphous olivine. The curves near the bottom of Fig. 11 represent those contributions to

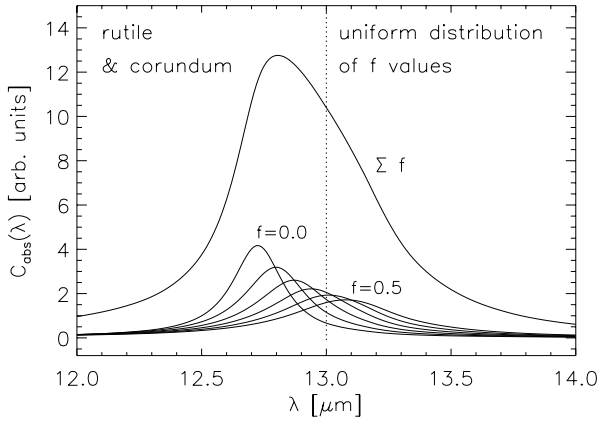


Fig. 12. The absorption efficiency of core-mantle-grains composed of rutile and corundum, the core volume fraction being uniformly distributed between 0 and 50%.

Σf for which $0.75 \leq f \leq 1$. The Σf curve peaks at $12.83 \mu\text{m}$, which is very close to the peak position of pure corundum of $12.72 \mu\text{m}$. To arrive at a peak position of $12.95 \mu\text{m}$, a distribution function biased towards $f \approx 0.85$ would have to be assumed.

To summarize, two rather arbitrary assumptions are necessary in order to reconcile the observed $13 \mu\text{m}$ feature with our calculations for corundum-silicate core-mantle-grains:

- (a) the presence of a large population of almost pure silicate grains;
- (b) a maximum of the distribution function of the core volume fractions near 0.85.

This can also be expressed in the following way: There have to be, on the one hand, many particles consisting of about 85% corundum to account for the observed band position of $12.95\text{--}13 \mu\text{m}$; on the other hand, there have to be about 10 times more particles consisting mainly of amorphous olivine to produce silicate bands comparable in strength to the $13 \mu\text{m}$ band. It seems to us that this is quite an artificial way of explaining the observed feature.

4.2. Rutile-corundum

As already mentioned, TiO_2 is considered a candidate for the prime condensate in oxygen-rich circumstellar dust shells. It is therefore not unlikely that core-mantle-grains composed of TiO_2 , $\alpha\text{-Al}_2\text{O}_3$ and other substances, form around long period variables. Using the methods described in Sect 4.1, we calculated C_{abs}/V for particles composed of rutile and corundum, again for different values of the core volume fraction. As is evident from Fig. 12, for uniformly distributed values of f , the peak position of C_{abs} is $12.8 \mu\text{m}$. On the other hand, for $0.3 \leq f \leq 0.4$, a spectral signature very well comparable in position to the observed $13 \mu\text{m}$ band profile emerges (see Fig. 14).

However, essentially the same objections as above have to be raised against this possible carrier of the $13 \mu\text{m}$ band. First, we cannot think of any physical mechanism that would cause the distribution function of the rutile core volume fractions to be biased towards 0.3–0.4; second, even if we assume a distribution

function yielding the ‘correct’ feature position, this feature will be shifted to longer wavelengths in case that a silicate mantle grows on top of the corundum mantle. The latter problem is discussed in more detail below.

4.3. Three-component-particles

Since there is no reason to assume that core-mantle-grains consist of two components only, it is of interest to calculate C_{abs} for three-component-particles. Unfortunately, it is not correct to simply apply Eq. (2) iteratively. Farafonov (1999) presented a general formalism to calculate the absorption efficiency of N-layered ellipsoids. For $N=3$ and spherical particles small compared to the wavelength, it reads:

$$\frac{C_{abs}}{V} = \frac{3\pi}{\lambda} \Im(\alpha) \quad (4)$$

$$\alpha = \frac{A_2 - A_1}{A_2 + 2A_1} \quad (5)$$

$$\begin{pmatrix} A_1 \\ A_2 \end{pmatrix} = \begin{pmatrix} 1 & 1/3 \\ e_3 & (-2/3)e_3 \end{pmatrix} \times \begin{pmatrix} (1/3)(e_2 - 1) + 1 & (-2/9)(e_2 - 1)/v_2 \\ -(e_2 - 1)v_2 & (2/3)(e_2 - 1) + 1 \end{pmatrix} \times \begin{pmatrix} (1/3)(e_1 - 1) + 1 \\ -(e_1 - 1)v_1 \end{pmatrix} \quad (6)$$

where $e_j = \varepsilon_j/\varepsilon_{j+1}$ is the relative dielectric function (for $j=3$, $e_j = \varepsilon_j$) and v_j is the volume fraction of the j th sphere with respect to the total particle volume.

In spite of the relative complexity of this formalism, its result for a particle consisting of rutile core, a corundum and a silicate mantle can be summarized in a few words. The shift of the $12.7 \mu\text{m}$ corundum emissivity maximum towards $14 \mu\text{m}$ by a silicate mantle also occurs in case of a rutile-corundum-core. If we consider, for example, a core-mantle grain composed of 40 volume percents of TiO_2 and 60% $\alpha\text{-Al}_2\text{O}_3$ – having an emissivity peak position of $13.0 \mu\text{m}$ –, then coating it with large silicate mantles will shift the peak to wavelengths of $14.2\text{--}14.4 \mu\text{m}$ (see Fig. 13).

5. Conclusions

It is obvious that one could think of much more species especially of core-mantle-grains and compare their emissivity with the $13 \mu\text{m}$ band profile. However, it has been our intention to take into account only those substances (and simple combinations of them) which are expected to form in oxygen-rich circumstellar outflows.

In Table 2, position and width of the average $13 \mu\text{m}$ feature that we have derived from our sample spectra are confronted with the corresponding values for the grain species that are more or less likely to account for it. Here, only spherical particle shapes are considered. Fig. 14 presents a part of this comparison graphically.

It is immediately evident from Table 2 that among the one-component-grains spinel’s emissivity curve is most similar to

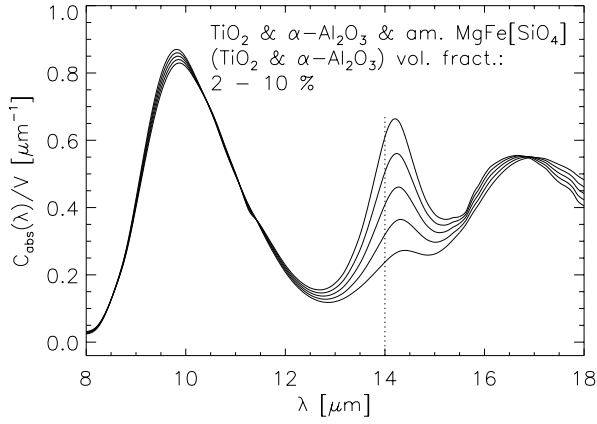


Fig. 13. C_{abs}/V for three-component grains consisting of a rutile core, a corundum-, and, additionally, a silicate-mantle. The rutile core fills 40% of the volume of the rutile-corundum-grain, which in turn amounts 2–10% of the whole particle volume.

Table 2. Comparison of the properties of the average 13 μm band profile with those of possible carrier substance

substance	λ_{peak} [μm]	FWHM [μm]	other C_{abs} -max. [and comments]
observed	13.0	0.6	16.8 (, 15.8)
carrier			
corundum	12.7	0.3	19.9, 21.0
spinel	12.95	0.6	16.8
rutile	13.4	1.2	22.9, 27.4
am. SiO ₂	12.3	1.3	8.9 [main], 20.5
rcor40	13.0	0.6	[rutile-corundum $f=0.4$]
csil85	12.95	0.5	[corundum-olivine $f=0.85$]
rcor0-100	12.8	0.6	[rutile-corundum Σf]
csil0-100	12.8	0.6	[corundum-olivine Σf]

the observed band profile. Corundum produces a feature at too small a wavelength, whereas the opposite is true for rutile. An additional argument for spinel being the carrier of the 13 μm feature is the coincidence of its 16.8 μm secondary feature with a spectral signature in the residual emission profile. The latter could also be due to MgO. This possibility can be ruled out if a tight correlation between the strength of both features exists, which has to be verified in a future investigation.

Core-mantle-grains composed of rutile and corundum or of corundum and amorphous olivine also agree in their optical properties with the 13 μm feature carrier, though in a limited range of core volume fractions only. The latter limitation clearly makes them less promising candidates.

Since for spinel and rutile, relatively few sets of optical constants exist (see Henning et al. 1999), it seems desirable to make additional laboratory measurements of these substances.

Acknowledgements. We thank the referee Dr. A. Omont and Dr. T. Lebzelter for valuable comments. FK's work was supported by APART (Austrian Programme for Advanced Research and Technology) from the Austrian Academy of Sciences and by the Österreichische Nationalbank under Jubiläumsfonds-project number 6876. This research was also supported by the Österreichische Nationalbank under Jubi-

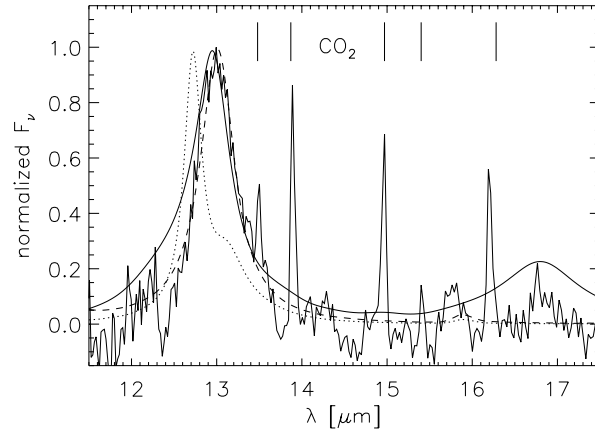


Fig. 14. The average 13 μm band profile compared to normalized C_{abs} -profiles of three possible carrier substances. The dotted line represents corundum, the dashed one a grain composed of a rutile core (40 vol. perc.) and a corundum mantle, and the solid line represents spinel.

läumsfonds-project number 6980. The ISO Spectral Analysis Package (ISAP) is a joint development by the LWS and SWS Instrument Teams and Data Centers. Contributing institutes are CESR, IAS, IPAC, MPE, RAL and SRON.

References

- Barker A.S. Jr., 1963, Phys. Review 132, 1474
 Bagnulo S., 1996, Thesis, Univ. of Belfast, p. 91
 Begemann B., Dorschner J., Henning T., et al., 1999, ApJ 476, 199
 Bergmann P., Kerschbaum F., Olofsson H., 1999, A&A, in press
 Bohren C.F., Huffman D.R., 1983, Absorption and Scattering of Light by Small Particles. John Wiley, New York
 Dorschner J., Begemann B., Henning T., Jäger C., Mutschke H., 1995, A&A 300, 503
 Farafonov V.G., 1999, Optics & Spectroscopy, submitted
 Gail H.-P., Sedlmayr E., 1998, In: Chemistry and Physics of Molecules and Grains in Space. Faraday Discussion no. 109, The Faraday Division of the Royal Society of Chemistry, London, p. 303
 Gervais F., Piriou B., 1974, J. Phys. C. - Solid St. Phys. 7, 2374
 Gervais F. 1974, Piriou B., 1975, Revue Internationale des Hautes Températures et des Réfractaires 12, 58
 Gervais F., 1991, In: Palik E.D. (ed.) Handbook of Optical Constants of Solids II, Academic Press, Boston, p. 761
 de Graauw T., Haser L.N., Beintema D.A., et al., 1996, A&A 315, L49
 Hackwell J.A., 1972, A&A 21, 239
 Henning T., Begemann B., Mutschke H., Dorschner J., 1995, A&AS 112, 143
 Henning T., Mutschke H., 1997, A&A 327, 743
 Henning T., Il'in V.B., Krivova N.A., et al., 1999, WWW database of optical constants for astronomy. A&AS 136, 405
 Henning T., Mutschke H., 1999, In: Sitko M.L., Sprague A.L., Lynch D.K. (eds.) Thermal Emission Spectroscopy and Analysis of Dust, Discs and Regoliths. ASP Conference Series, in press
 Hron J., Aringer B., Kerschbaum F., 1997, A&A 322, 280
 Jeong K.S., Winters J.M., Sedlmayr E., 1999, In: Le Bertre T., Lèbre A., Waelkens C. (eds.) Asymptotic Giant Branch Stars. Proc. IAU Symp. 191, ASP Conf. Ser. p. 233
 Justanont K., Feuchtgruber H., de Jong T., et al., 1998, A&A 330, L17-L20

- Kahane C., Jura M., 1994, A&A 290, 183
Kerschbaum F., Hron J., 1992, A&A 263, 97
Kerschbaum F., Hron J., 1994, A&AS 106, 397
Kerschbaum F., 1995, A&AS 113, 441
Kerschbaum F., Hron J., 1996, A&A 308, 489
Kerschbaum F., Olofsson H., Hron J., 1996, A&A 311, 273
Kerschbaum F., Olofsson H., Hron J., 1997, In: Sasselov D.D., Takeuti M. (eds.) Proc. of JD24, 23rd GA of the IAU, Universal Academy Press, Tokyo, p. 177
Kerschbaum F., Posch T., Aringer B., 1999, In: Hron J., Höfner S. (eds.) 2nd Austrian ISO Workshop, Institute of Astronomy, University of Vienna, p. 57
Knapp G.R., Young K., Lee E., Jorissen A., 1998, ApJS 117, 209
Koike C., Shibai H., 1998, ISAS Report No. 671, p. 17
Kozasa T., Sogawa H., 1997, Ap&SS 251, 165
Mutschke H., et al., 1998, A&A 333, 188
Nittler L.R., 1997, In: Bernatowicz T.J., Zinner E. (eds.) Astrophysical Implications of the Laboratory Study of Presolar Materials. AIP Conference Proceedings 402, p. 59
Onaka T., de Jong T., Willems F.J., 1989, A&A 218, 169
Ossenkopf V., Henning T., Mathis J.S., 1992, A&A 261, 567
Palik E.D., 1985–1998, In: Palik E.D. (ed.) Handbook of Optical Constants of Solids. 3 vols., Academic Press, Boston
Philipp H.R., 1985, In: Palik E.D. (ed.) Handbook of Optical Constants of Solids I, Academic Press, Boston, p. 749
Posch T., Kerschbaum F., 1999, In: Hron J., Höfner S. (eds.) 2nd Austrian ISO Workshop, Institute of Astronomy, University of Vienna, p. 39
Ribarsky M.W., 1985, In: Palik E.D. (ed.) Handbook of Optical Constants of Solids I, Academic Press, Boston, p. 795
Sloan G.C., LeVan P.D., Little-Marenin I.R., 1996, ApJ 463, 310
Sloan G.C., Price S.D., 1998, ApJS 119, 141
Speck A.K., 1998, Thesis, University College London
Tropf W.J., Thomas M.E., 1991, In: Palik E.D. (ed.) Handbook of Optical Constants of Solids II, Academic Press, Boston, p. 883
Worrell C.A., 1986, J. Mat. Science 21, 781